Journal of Power Sources 246 (2014) 783–787

Contents lists available at ScienceDirect

Journal of Power Sources

journal homepage: www.elsevier.com/locate/jpowsour

Short communication

Pyrophosphate $Na_2FeP_2O_7$ as a low-cost and high-performance positive electrode material for sodium secondary batteries utilizing an inorganic ionic liquid

Chih-Yao Chen [a], Kazuhiko Matsumoto [a], Toshiyuki Nohira [a,*], Rika Hagiwara [a,*], Yuki Orikasa [b], Yoshiharu Uchimoto [b]

[a] Graduate School of Energy Science, Kyoto University, Sakyo-ku, Kyoto 606-8501, Japan
[b] Graduate School of Human and Environmental Studies, Kyoto University, Sakyo-ku, Kyoto 606-8501, Japan

HIGHLIGHTS

- The performance of $Na_2FeP_2O_7$ positive electrode was evaluated at 363 K.
- NaFSA–KFSA inorganic ionic liquid was used as an electrolyte.
- The reversible capacity of $Na_2FeP_2O_7$ reaches 91 mA h g^{-1}.
- Capacity retention of 91% after 1000 cycles was demonstrated.
- Variations of Fe valence states and Fe–O bonds upon electrochemical cycling were studied by XAS.

ARTICLE INFO

Article history:
Received 11 June 2013
Accepted 9 August 2013
Available online 17 August 2013

Keywords:
Sodium secondary battery
$Na_2FeP_2O_7$
Positive electrode
Ionic liquid
Bis(fluorosulfonyl)amide

ABSTRACT

The electrochemical performance of a $Na_2FeP_2O_7$ positive electrode has been evaluated in an inorganic ionic liquid NaFSA–KFSA (FSA = bis(fluorosulfonyl)amide) at 363 K. The electrode delivers a reversible capacity of 91 mAh g^{-1} with excellent rate capability (59 mAh g^{-1} at 2000 mA g^{-1}) and a capacity retention of 91% over 1000 cycles, which facilitates the development of low-cost and high-safety sodium secondary batteries for large-scale energy storage applications. The average oxidation state of iron increases upon sodium extraction, as evidenced by the edge shift of an X-ray absorption spectroscopy analysis. According to an extended X-ray absorption fine structure analysis, the sodium extraction is accompanied by a shortening of Fe–O bonds.

1. Introduction

New and advanced materials for electrical energy storage are urgently required for the seamless integration of intermittent renewable energy resources in electricity grids [1–4]. To realize forthcoming large-scale battery systems, the balance between cost and performance will be essential [3,4]. Sodium secondary batteries are one of the most promising batteries for future stationary energy storage and popularly priced electric vehicles owing to the high abundance and low-cost of sodium *versus* lithium, coupled with the reasonably low Na^+/Na redox potential (−2.71 V vs. SHE) [5,6]. Despite the advantages and opportunities, sodium batteries exhibit lower energy density, inferior rate performance and poorer cyclability, as compared to lithium-ion batteries. Thus, the exploration and development of both electrode materials and electrolytes are crucial for future applications of sodium secondary batteries.

In lithium-ion batteries, polyanionic compounds are receiving growing attention because of the inherent stability of the polyanion group, thus providing a safety asset [7]. Moreover, polyanionic compounds which exchange multiple electrons per transition metal are particularly interesting due to the expectation for realizing a high specific energy [8]. From the viewpoints of cost and mass production, the search for polyanionic compounds containing naturally abundant Fe as a redox center is of timely significance [9].

* Corresponding authors. Tel.: +81 75 753 5822; fax: +81 75 753 5906.
E-mail addresses: nohira@energy.kyoto-u.ac.jp (T. Nohira), hagiwara@energy.kyoto-u.ac.jp (R. Hagiwara).

0378-7753/$ – see front matter © 2013 Elsevier B.V. All rights reserved.
http://dx.doi.org/10.1016/j.jpowsour.2013.08.027

This has led to intensive studies of olivine $LiFePO_4$ [10], the leading contender as the positive electrode for lithium-ion batteries. New compounds such as silicate (Li_2FeSiO_4) [11–13], fluorinated phosphate (Li_2FePO_4F) [14], and pyrophosphate $Li_2FeP_2O_7$ [15–17] have recently been identified to exhibit good electrochemical properties at favorable redox potentials. Compared to well-established materials for lithium-ion technology, however, few iron-based polyanionic compounds have been characterized and tested for sodium secondary batteries [9,18–20]. For example, three Na ions can be extracted from the mixed-polyanion compound $Na_4Fe_3(PO_4)_2(P_2O_7)$, resulting in a capacity of 129 mAh g^{-1} with an average voltage of 3.2 V [9]. Very recently, $Na_2FeP_2O_7$ was shown to have a reversible capacity of 82 mAh g^{-1} in $NaClO_4$ dissolved in propylene carbonate (PC) at room temperature [20].

Ionic liquids are promising electrolytes for improving the safety and reliability of batteries, owing to their high thermal and electrochemical stabilities, as demonstrated for lithium-ion batteries [21,22]. Concerning sodium batteries, however, most research efforts from the scientific community have targeted electrode materials, whereas the adoption of ionic liquid electrolytes for sodium batteries received less attention. Thus, investigating the electrochemical performance of polyanionic compounds such as $Na_2FeP_2O_7$ as positive electrode materials in ionic liquids is worthwhile. Regarding negative electrode materials for sodium batteries, comprehensive characterization and testing have proven that hard carbons as the first-generation anode of choice [23–25]. However, the Na-intercalated hard carbon (Na_xC) exhibits higher reactivity toward organic electrolytes than Li_xC_6, raising imperative concerns about the stability of the organic electrolyte [26]. In addition, their electrochemical performance strongly depends on the electrolyte used [27]; therefore, the use of ionic liquid electrolytes is also interesting for the performance of negative electrodes.

A new class of intermediate-temperature ionic liquids consisting of alkali metal cations and bis(fluorosulfonyl)amide anions (FSA) has recently been developed [28–30]. Among them, the NaFSA–KFSA system is an especially promising electrolyte for sodium secondary batteries [31]. In contrast to conventional ionic liquids that usually contain expensive organic cations, NaFSA and KFSA are simple inorganic compounds. In addition, opposite to TFSA (TFSA = bis(trifluoromethylsulfonyl)) salts, FSA salts can be synthesized without the costly electrofluorination process, thus potentially enabling reasonable prices in the near future. So far, encouraging results have been obtained for $NaCrO_2$ positive electrode [31,32] and Sn negative electrode [33,34] in NaFSA–KFSA at 353–363 K.

In this context, the combination of low-cost $Na_2FeP_2O_7$ electrode materials built from abundant elements with affordable NaFSA–KFSA ionic liquids is extremely interesting to study. Herein, the electrochemical performance of a $Na_2FeP_2O_7$ positive electrode was first evaluated by a galvanostatic charge–discharge test in the NaFSA–KFSA ionic liquid at 363 K. Second, the mechanism of sodium extraction from $Na_2FeP_2O_7$ was studied by ex-situ X-ray absorption spectroscopy (XAS).

2. Experimental

Sodium iron pyrophosphate $Na_2FeP_2O_7$ was synthesized by a two-step solid-state method. The starting materials, Na_2CO_3 (Wako, purity 99.8%), $FeC_2O_4 \cdot 2H_2O$ (Wako, purity 99%) and $(NH_4)_2HPO_4$ (Wako, purity >99%), were thoroughly mixed by wet planetary ball-milling in acetone for 8 h. After evaporating the acetone, the mixture was ground and was initially heated at 573 K for 6 h. The calcined sample was reground and heated again at 873 K for 12 h. Argon flow was used to suppress the oxidation of Fe^{2+} during the heat treatments. The structure of the as-synthesized materials was characterized by powder X-ray diffraction (XRD) using a Rigaku SmartLab instrument equipped with Cu-Kα radiation (40 kV and 30 mA).

The working electrode was prepared by mixing as-synthesized $Na_2FeP_2O_7$, acetylene black (AB) conductive additive and polytetrafluoroethylene (PTFE) as binder in a weight ratio of 75:20:5. Metallic sodium discs (Aldrich, purity 99.85%) were pressed onto nickel current collectors and used as reference and counter electrodes. Electrochemical measurements were carried out in a NaFSA–KFSA (56:44 molar ratio) ionic liquid with glass microfiber filters (Whatman GF/A) in between the electrodes as separators. NaFSA and KFSA (Mitsubishi Materials Electronic Chemicals) were dried under vacuum at 353 K for 24 h in advance. The separator was impregnated under vacuum with the electrolyte at 363 K for 2 days prior to the test. The electrochemical tests were conducted with a Bio-Logic VSP potentiostat. For the galvanostatic intermittent titration technique (GITT) experiments, the cells were charge–discharged at a current density of 4.85 mA g^{-1} (C/20 rate) for 1 h, and then the circuit was opened until the voltage shift below 10 mV h^{-1}. In this paper, the theoretical capacity of $Na_2FeP_2O_7$ is defined as 97 mAh g^{-1}, corresponding to one-electron transfer.

XAS experiments were performed at the beam line BL01B1 of the synchrotron radiation facility in SPring-8 (Hyogo, Japan). Fe *K*-edge spectra were measured in a transmission mode using a Si(111) monochromator. Fe metal foil was used for the calibration of the absorption energy scale. The experimental data of all samples were analyzed with the program REX-2000. The backscattering phases and the amplitude were theoretically calculated by the code FEFF8 [35]

3. Results and discussion

The XRD pattern of the prepared $Na_2FeP_2O_7$ depicted in Fig. S1 is consistent with the pattern reported in the literature [19]. The $Na_2FeP_2O_7$ compound is isostructural with $Na_2CoP_2O_7$-rose, stabilizing into a triclinic *P*-1 cell [36]. The crystal structure consists of the corner-sharing FeO_6 octahedra and bridging pyrophosphate groups, thereby creating large tunnel structures along specific directions for facile Na ion migration. Like many pyrophosphate compounds with high thermal stability, $Na_2FeP_2O_7$ showed negligible weight loss and no indication of phase transformation up to 823 K [19]. Thus, $Na_2FeP_2O_7$ is considered stable at the present measurement temperature (363 K). Scanning electron microscopy of as-synthesized $Na_2FeP_2O_7$ particles revealed irregular morphology with diameter ranging from 0.1 to 1 μm and partial aggregation (Fig. 1). Tailoring the particle morphology in solid-state synthesis is challenging because experiments conducted at high temperature inevitably lead to particle growth and coarsening.

The initial three cycling profiles of $Na_2FeP_2O_7$ (at a current density of 10 mA g^{-1}) are displayed in Fig. 2(a). A shift of the plateau potential was observed from the first to the subsequent charging processes. The subsequent charge–discharge profiles coincided, indicating no major structural change after the first charging. The electrochemical activity centered around 3.0 V is consistent with the reported value, indicating the feasibility of the NaFSA–KFSA ionic liquid as electrolyte [19,20]. A reversible capacity of 91 mAh g^{-1} was observed, corresponding to approximately 94% of the theoretical capacity (97 mAh g^{-1}). The observed irreversible potential profile for the first charge has also been reported for $Li_2FeP_2O_7$ and Li_2FeSiO_4 [11–13,15]. For Li_2FeSiO_4, the observed decrease in the plateau potential by 0.2–0.7 V during the first oxidation was explained by structural ordering processes including the transition from a short-range ordered solid-solution to a more stable phase [11–13]. A similar structural rearrangement is thought

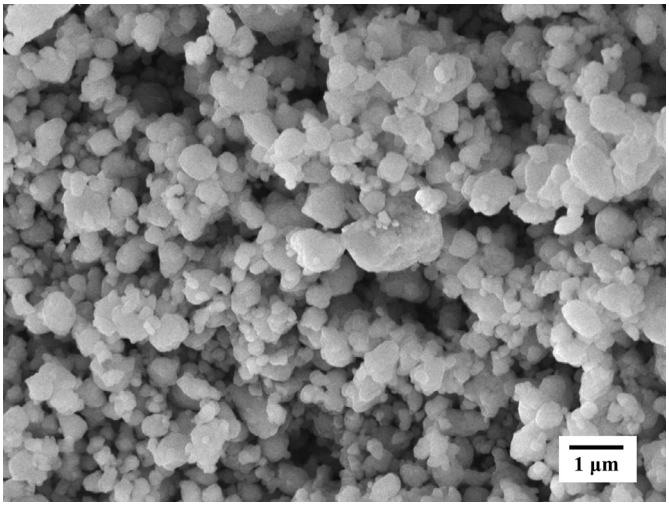

Fig. 1. SEM image of as-synthesized $Na_2FeP_2O_7$.

to occur in the present study. The working voltage of $Na_2FeP_2O_7$ is similar to that of the Fe^{3+}/Fe^{2+} couple in Na_2FePO_4F (3.0 V) [18] and higher than that of olivine $NaFePO_4$ (2.7 V) [37].

Charge–discharge curve close to the thermodynamic equilibrium was obtained from the galvanostatic intermittent titration technique (GITT) in which each intercalation/deintercalation process is followed by a relaxation period allowing material homogenization. The GITT profiles measured at 4.85 mA g^{-1} (C/20 rate) during the first two cycles are presented in Fig. 2(b). The shape of the curves is very similar to the one obtained under continuous charge–discharge conditions, suggesting facile electrode kinetics with a small overpotential, especially for the Na intercalation process. After the structural rearrangement upon the first charging described above, two distinct regions were observed in the charging profile: a low-voltage region (2.5–3.1 V) and a high-voltage region (>3.1 V). The former region shows a sloping voltage profile with small overpotential, suggesting solid-solution formation; whereas, the latter region exhibits a flat voltage plateau with large overpotential, which is a characteristic feature for the biphasic transition [38]. Results of cyclic voltammetry (CV) consistently exhibit current peaks at the relevant locations (Fig. S2, Supplementary data). The finding that two kinds of reactions are associated within whole Na deintercalation process is consistent with the predication based on the DFT calculations reported recently [19]. Na ions occupy four crystallographically different sites within $Na_2FeP_2O_7$ [20], and the large overpotential observed in the high-voltage region may be ascribed to the extraction of Na ions located in small channels. These Na ions seem to be rarely re-intercalated because the reversible amount of Na is below 1 mol per formula. The comparison of the XRD patterns of pristine, fully desodiated, and fully sodiated $Na_2FeP_2O_7$ (Fig. S3, Supplementary data) indicates that a stable overall framework of $Na_2FeP_2O_7$ and a first-order biphasic transition.

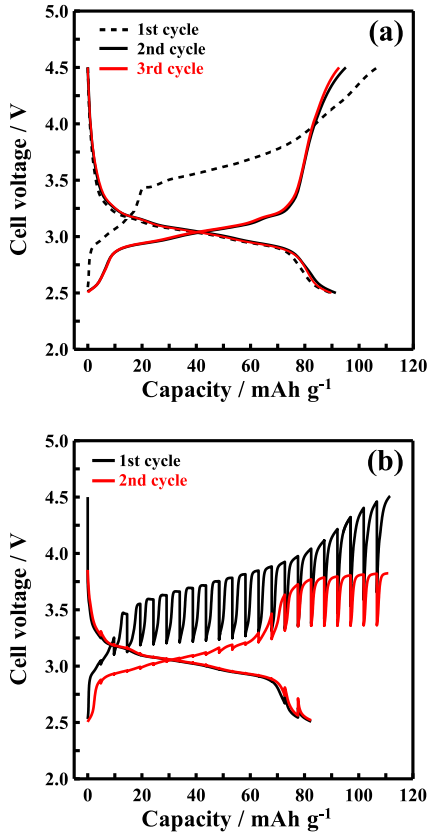

Fig. 2. (a) Galvanostatic charge–discharge curves of the initial three cycles for the Na/NaFSA–KFSA/$Na_2FeP_2O_7$ cell at a current density of 10 mA g^{-1} in the voltage range of 2.5–4.5 V at 363 K. (b) GITT curves measured at 4.85 mA g^{-1} (C/20 rate) of the initial two cycles at 363 K.

The rate capability of the $Na_2FeP_2O_7$ electrode is shown in Fig. 3. The cell was charged to 4.5 V at a constant current of 5 mA g^{-1} and then discharged to 2.5 V at various current densities. Approximately 66% and 52% of the maximum capacity at 5 mA g^{-1} (90 mAh g^{-1}) were observed at 2000 and 3000 mA g^{-1}, respectively. The discharge capacity is still clearly discernible up to at current density of 4000 mA g^{-1}. The rate capability of $Na_2FeP_2O_7$ cycled in the NaFSA–KFSA electrolyte at 363 K is significantly better than those obtained in organic electrolytes at room temperature [19,20]. Moreover, this high rate capability is comparable to that of state-of-the-art electrode materials for lithium-ion batteries. For example, $LiFePO_4$, a common lithium-ion positive electrode, exhibited about 80% of its theoretical capacity at a 20 C rate [39,40]. The prominent rate capability obtained here can be attributed to improved kinetics at the elevated temperature and the large-tunnel structure of $Na_2FeP_2O_7$. The cycling performance of $Na_2FeP_2O_7$ at 100 mA g^{-1} (*ca.* 1 C) is shown in Fig. 4. It retains 91% of the initial capacity after 1000 cycles. The average coulombic efficiency over the whole experiment was as high as 99.9%. The cyclability of $Na_2FeP_2O_7$ electrodes has also been tested in organic electrolytes, but the results of only limited cycles (<100 cycles) are reported [19,20]. It should be noted that this excellent cycle performance

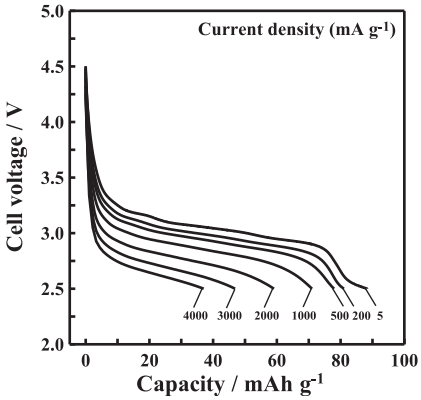

Fig. 3. Discharge curves of the $Na_2FeP_2O_7$ positive electrode at various current densities at 363 K. The charging up to 4.5 V was always conducted at 5 mA g^{-1}.

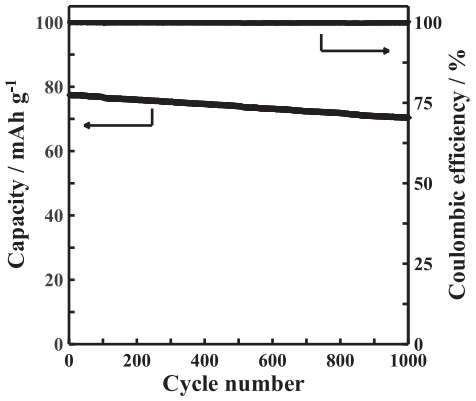

Fig. 4. Cycling performance and coulombic efficiency of the $Na_2FeP_2O_7$ positive electrode at 100 mA g^{-1} and 363 K. Cut-off voltage: 2.5–4.0 V.

was achieved using the $Na_2FeP_2O_7$ electrodes without optimization such as carbon coating. The present result demonstrates that the robust framework and structural integrity of pyrophosphate allows intercalation/deintercalation of Na ions. Moreover, the high stability of $Na_2FeP_2O_7$ can be fully utilized in conjunction with a chemically stable electrolyte such as the NaFSA–KFSA ionic liquid.

Although the inductive effect generated by the polyanionic groups leads to a higher operating voltage compared to simple oxides [10], the polyanionic groups simultaneously isolating the valence electrons of transition metals often lead to the observed low electronic conductivities [41]. Consequently, specific material treatments such as carbon-coating [42] and/or resorting to nanoparticles are usually necessary to achieve a high electrochemical performance [7]. However, many manufacturing challenges still prevent achieving high-quality products with high consistency [43]. Furthermore, the volumetric energy density (Wh L^{-1}) suffers greatly from the size minimization as most of the nano-sized materials do not have the practical packing scheme yet [44]. In addition to the ease and scalability of the present solid-state synthesis, the prepared samples possess relatively large particle size, which improves the material packing density. The moderately elevated operating temperature and high stability of the NaFSA–KFSA ionic liquid also suppress the need for electrode optimization.

XAS provided a deep insight into the change of electronic and local structural properties of $Na_2FeP_2O_7$ electrodes upon sodium intercalation/deintercalation. The normalized Fe *K*-edge X-ray absorption near-edge structure (XANES) spectra of the pristine, charged, and discharged $Na_2FeP_2O_7$ are displayed in Fig. 5. The XANES spectra of the four investigated samples differ both in the overall shape and the energy position of the main peak. Specifically, the main edge shows a strong shift (*ca.* 4.0 eV) toward higher energy as the charging voltage increases, and vice versa (for the negative shift). This shift of the main edge is explained by screening effects of the 1s electrons leading to a stronger bond in the Fe^{3+} state than that in the Fe^{2+} state, suggesting that the reversible Fe^{3+}/Fe^{2+} redox activity is involved in the electrochemical desodiation/sodiation reaction of $Na_2FeP_2O_7$ [45,46]. The pre-edge region of the XAS spectra is shown in the inset of Fig. 5. The different shapes of the pre-edge resonance for the pristine and charged/discharged $Na_2FeP_2O_7$ samples indicate the irreversible changes in the local environment of Fe in $Na_2FeP_2O_7$ upon electrochemical cycling. The higher pre-edge intensity of the discharged states (sample (d)) compared to that of the charged states (samples (b) and (c)) implies that the coordination around Fe cations deviate from the normal octahedral coordination more severely in the sodiated state than in the desodiated state. Although the electrode was charged up to 4.8 V to explore the possibility of extracting the second Na in $Na_2FeP_2O_7$, no Fe oxidation above +3 was detected (Fig. S4, Supplementary data). At this point, we can state if this limitation is due to the kinetics or thermodynamics of $Na_2FeP_2O_7$. A more detailed investigation is currently underway.

Fig. 6 shows the radial structure functions for the pristine and charged/discharged $Na_2FeP_2O_7$ samples, which have been obtained from Fourier transform (FT) of the extended X-ray absorption fine structure (EXAFS) oscillations. The simulation of the k^3-weighted Fe *K*-edge EXAFS spectra (Fig. S5, Supplementary data) for the present samples was performed using a limited *k* range (2.2–10.7 $Å^{-1}$) to minimize noise. The radial structure function reveals the scattering contribution of the different atomic shells around the Fe atoms. The first strong peak represents the octahedrally coordinated Fe–O shell, followed by several weaker peaks corresponding to Fe–P and Fe–Fe (not clear in some cases) correlations, respectively. The interatomic distances and corresponding Debye–Waller factors of the samples are shown in Supplementary data (Table S1, Supplementary data). A decrease of the average Fe–O bond from 2.106 Å (pristine) to 1.979 Å (4.0 V) upon Na extraction is observed, which can be attributed to the oxidation of Fe^{2+} to smaller Fe^{3+} ions as a result of charge compensation. Although the valence state of Fe at the end of discharge (2.7 V) is close to that in the pristine sample, the Fe–O bond length differs by 0.092 Å. Therefore, the EXAFS results verify the structural rearrangement of $Na_2FeP_2O_7$ during the initial desodiation, which is consistent with the variation of the charge–discharge curves (Fig. 2).

Large-scale battery systems for transportation applications or stationary storage clearly impose more challenging standards in

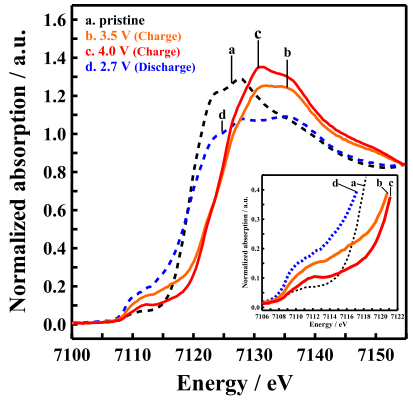

Fig. 5. Fe *K*-edge XANES spectra of (a) pristine $Na_2FeP_2O_7$ and $Na_2FeP_2O_7$ electrodes (b) charged to 3.5 V, (c) charged to 4.0 V, and (d) discharged to 2.7 V. Pre-edge region of the XAS spectra (inset).

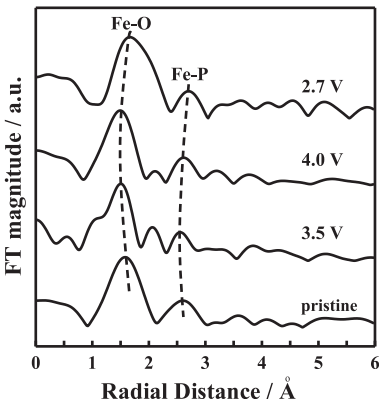

Fig. 6. Fourier transformation of Fe *K*-edge EXAFS of pristine $Na_2FeP_2O_7$ and $Na_2FeP_2O_7$ electrodes at different stages of charging/discharging.

various aspects. Several important performance characteristics such as power density, life cycle, and safety are principally determined by electrolytes. Accordingly, their continuous improvement and innovation are indeed critical to success. Our strategy of combining iron-based phosphate $Na_2FeP_2O_7$ with the intermediate-temperature ionic liquid NaFSA–KFSA provides a well-balanced solution for current challenges, as demonstrated in this study. The evidently excellent kinetics of the positive electrode at elevated temperature obviates the need for carbon-coating or nanosizing, which enables lowering the electrode processing cost.

4. Conclusions

Sodium iron pyrophosphate $Na_2FeP_2O_7$ was synthesized via a simple solid-state reaction. The $Na_2FeP_2O_7$ positive electrode showed competent electrochemical properties in the NaFSA–KFSA ionic liquid at 363 K: a reversible capacity of 91 mAh g^{-1} at 10 mA g^{-1}, an excellent rate capability of 59 mAh g^{-1} at 2000 mA g^{-1}, and a surprisingly high capacity retention of 91% after 1000 cycles. XAS studies confirm the reversible change in the Fe oxidation state accompanying a variation of Fe–O bond length upon electrochemical cycling. Further improvement in synthesis and electrode fabrication, e.g., optimization of the type of conductive additive or its content, can certainly enhance the electrochemical performance of this material. The combination of economic positive electrode materials built from abundant elements such as Fe, P, and Na with the safe, purely inorganic ionic liquid electrolytes will pave the way for the large-scale sodium secondary batteries.

Acknowledgments

This study was partly supported by the Advanced Low Carbon Technology Research and Development Program (ALCA) of the Japan Science and Technology Agency (JST) and by the program “Elements Strategy Initiative to Form Core Research Center” (since 2012) of the Ministry of Education Culture, Sports, Science and Technology, Japan (MEXT).

Appendix A. Supplementary data

Supplementary data related to this article can be found at http://dx.doi.org/10.1016/j.jpowsour.2013.08.027.

References

[1] A.S. Arico, P. Bruce, B. Scrosati, J.-M. Tarascon, W. Van Schalkwijk, Nat. Mater. 4 (2005) 366–377.
[2] M. Armand, J.-M. Tarascon, Nature 451 (2008) 652–657.
[3] Z.G. Yang, J.L. Zhang, M.C.W. Kintner-Meyer, X.C. Lu, D.W. Choi, J.P. Lemmon, J. Liu, Chem. Rev. 111 (2011) 3577–3613.
[4] J. Liu, J.G. Zhang, Z.G. Yang, J.P. Lemmon, C. Imhoff, G.L. Graff, L.Y. Li, J.Z. Hu, C.M. Wang, J. Xiao, G. Xia, V.V. Viswanathan, S. Baskaran, V. Sprenkle, X.L. Li, Y.Y. Shao, B. Schwenzer, Adv. Funct. Mater. 23 (2013) 929–946.
[5] Y.H. Lu, L. Wang, J.G. Cheng, J.B. Goodenough, Chem. Commun. 48 (2012) 6544–6546.
[6] S.W. Kim, D.H. Seo, X.H. Ma, G. Ceder, K. Kang, Adv. Energy Mater. 2 (2012) 710–721.
[7] Z.L. Gong, Y. Yang, Energy Environ. Sci. 4 (2011) 3223–3242.
[8] G. Hautier, A. Jain, H. Chen, C. Moore, S.P. Ong, G. Ceder, J. Mater. Chem. 21 (2011) 17147–17153.
[9] H. Kim, I. Park, D.H. Seo, S. Lee, S.W. Kim, W.J. Kwon, Y.U. Park, C.S. Kim, S. Jeon, K. Kang, J. Am. Chem. Soc. 134 (2012) 10369–10372.
[10] A. Padhi, K. Nanjundaswanmy, J.B. Goodenough, J. Electrochem. Soc. 144 (1997) 1188–1194.
[11] D. Rangappa, K.D. Murukanahally, T. Tomai, A. Unemoto, I. Honma, Nano Lett. 12 (2012) 1146–1151.
[12] A. Nyten, A. Abouimrane, M. Armand, T. Gustafsson, J.O. Thomas, Electrochem. Commun. 7 (2005) 156–160.
[13] Y. Zhao, J.X. Li, N. Wang, C.X. Wu, Y.H. Ding, L.H. Guan, J. Mater. Chem. 22 (2012) 18797–18800.
[14] B.L. Ellis, W.R.M. Makahnouk, Y. Makimura, K. Toghill, L.F. Nazar, Nat. Mater. 6 (2007) 749–753.
[15] S. Nishimura, M. Nakamura, R. Natsui, A. Yamada, J. Am. Chem. Soc. 132 (2010) 13596–13597.
[16] D. Shimizu, S. Nishimura, P. Barpanda, A. Yamada, Chem. Mater. 24 (2012) 2598–2603.
[17] H. Kim, S. Lee, Y.U. Park, H. Kim, J. Kim, S. Jeon, K. Kang, Chem. Mater. 23 (2011) 3930–3937.
[18] Y. Kawabe, N. Yabuuchi, M. Kajiyama, N. Fukuhara, T. Inamasu, R. Okuyama, I. Nakai, S. Komaba, Electrochem. Commun. 13 (2011) 1225–1228.
[19] H. Kim, R.A. Shakoor, C. Park, S.Y. Lim, J.S. Kim, W. Cho, K. Miyasaka, R. Kahraman, Y. Jung, J.W. Choi, Adv. Funct. Mater. 23 (2013) 1147.
[20] P. Barpanda, T. Ye, S. Nishimura, S.C. Chung, Y. Yamada, M. Okubo, H.S. Zhou, A. Yamada, Electrochem. Commun. 24 (2012) 116–119.
[21] M. Armand, F. Endres, D.R. MacFarlane, H. Ohno, B. Scrosati, Nat. Mater. 8 (2009) 621–629.
[22] S. Seki, Y. Kobayashi, H. Miyashiro, Y. Ohno, A. Usami, Y. Mita, M. Watanabe, N. Terada, Chem. Commun. (2006) 544–545.
[23] D.A. Stevens, J.R. Dahn, J. Electrochem. Soc. 147 (2000) 1271–1273.
[24] S. Komaba, W. Murata, T. Ishikawa, N. Yabuuchi, T. Ozeki, T. Nakayama, A. Ogata, K. Gotoh, K. Fujiwara, Adv. Funct. Mater. 21 (2011) 3859–3867.
[25] M.D. Slater, D. Kim, E. Lee, C.S. Johnson, Adv. Funct. Mater. 23 (2013) 947–958.
[26] X. Xia, M.N. Obrovac, J.R. Dahn, Electrochem. Solid-State Lett. 14 (2011) A130–A133.
[27] A. Ponrouch, E. Marchante, M. Courty, J.-M. Tarascon, M.R. Palacin, Energy Environ. Sci. 5 (2012) 8572–8583.
[28] K. Kubota, T. Nohira, T. Goto, R. Hagiwara, Electrochem. Commun. 10 (2008) 1886–1888.
[29] K. Kubota, T. Nohira, R. Hagiwara, J. Chem. Eng. Data 55 (2010) 3142–3146.
[30] K. Kubota, T. Nohira, R. Hagiwara, Electrochim. Acta 66 (2012) 320–324.
[31] A. Fukunaga, T. Nohira, Y. Kozawa, R. Hagiwara, S. Sakai, K. Nitta, S. Inazawa, J. Power Sources 209 (2012) 52–56.
[32] C.Y. Chen, K. Matsumoto, T. Nohira, R. Hagiwara, A. Fukunaga, S. Sakai, K. Nitta, S. Inazawa, J. Power Sources 237 (2013) 52–57.
[33] T. Yamamoto, T. Nohira, R. Hagiwara, A. Fukunaga, S. Sakai, K. Nitta, S. Inazawa, J. Power Sources 217 (2012) 479–484.
[34] T. Yamamoto, T. Nohira, R. Hagiwara, A. Fukunaga, S. Sakai, K. Nitta, S. Inazawa, J. Power Sources 237 (2013) 98–103.
[35] J.J. Rehr, C. Albers, Rev. Mod. Phys. 72 (2000) 621–654.
[36] E. Erragh, A. Boukhari, B. Elouadi, E.M. Holt, J. Crystallogr. Spectrosc. Res. 21 (1991) 321–326.
[37] S.M. Oh, S.T. Myung, J. Hassoun, B. Scrosati, Y.K. Sun, Electrochem. Commun. 22 (2012) 149–152.
[38] R. Berthelot, D. Carlier, C. Delmas, Nat. Mater. 10 (2011) 74–80.
[39] B. Kang, G. Ceder, Nature 458 (2009) 190–193.
[40] G. Ceder, B. Kang, J. Power Sources 194 (2009) 1024–1028.
[41] S.Y. Chung, J.T. Bloking, Y.M. Chiang, Nat. Mater. 1 (2002) 123–128.
[42] N. Ravet, Y. Chouinard, J.F. Magnan, S. Besner, M. Gauthier, M. Armand, J. Power Sources 97–98 (2001) 503–507.
[43] J.J. Wang, X.L. Sun, Energy Environ. Sci. 5 (2012) 5163–5185.
[44] B. Xu, D.N. Qian, Z.Y. Wang, Y.S. Meng, Mater. Sci. Eng., R 73 (2012) 51–65.
[45] O. Haas, A. Deb, E.J. Cairns, A. Wokaun, J. Electrochem. Soc. 152 (2005) A191–A196.
[46] A. Deb, U. Bergmann, E.J. Cairns, S.P. Cramer, J. Synchrotron Radiat. 11 (2004) 497–504.